An Electrochemical Investigation of the EDTA Influence on the Cobalt-Manganese Electrodeposition in Aqueous Chloride Electrolytes

Huihui Zhang[1,], Juntao Yuan[2], Ming Zhu[1]*

[1] School of Materials Science and Engineering, Xi'an University of Science and Technology, Xi'an 710054, China
[2] State Key Laboratory of Performance and Structural Safety for Petroleum Tubular Goods and Equipment Materials, Tubular Goods Research Institute of CNPC, Xi'an 710077, China
[*]E-mail: hhzhang_xust@163.com

After subsequent proper heat treatment, a Co-Mn alloy coating is potentially a protective and conductive coating on ferritic stainless steel interconnects in solid oxide fuel cells. In this paper, we use electrochemical measurements to report the effects of EDTA (disodium ethylenediaminetetraacetate) in a chloride electrolyte on the Co-Mn electrodeposition process. The addition of EDTA to the chloride electrolyte significantly shifts the reduction reaction potential of cobalt in a more negative direction while slightly altering the discharging potential of manganese and most importantly, shortening to a great extent the discharge potential difference between Co^{2+} and Mn^{2+}. Also, it is crucial to control the $[Co^{2+}]$/[EDTA] ratio to form completely complexed cobalt ions and a very small amount of complexed manganese ions, and thus to promote the deposition of the Co-Mn alloy. The addition of EDTA to the chloride electrolyte is a promising way to prepare a Co-Mn alloy coating via electrodeposition.

1. INTRODUCTION

In recent years, the operating temperature of solid oxide fuel cells has been reduced to 600-800 °C, so that relatively cheap chromia-forming steels, such as ferritic stainless steels, can be used as interconnects to replace costly ceramics [1,2]. However, there are two important drawbacks hindering

the long-term application of chromia-forming metallic interconnects: an increase in area specific resistance and poisoning of the porous cathode [3,4].

Much effort has been made to prepare Cr-free protective coatings to reduce chromium volatilization and to achieve excellent electrical conductivity. In particular, Co-Mn spinel coatings have received wide attention because of their advantages. Specifically, they have of good electrical conductivity, an excellent coefficient of thermal expansion that matches that of ferritic stainless steel interconnects and other components such as the anode and cathode, and their high capability for absorbing chromium species migrating from the chromia-rich scale [5,6]. Slurry (including spraying [7], screen printing [8], and plasma spraying [9]) and electrodeposition methods [10-13] have mainly been used to prepare spinel coatings on stainless steel substrates. Although slurry coating processes are simple for producing thick coatings, the coatings are usually porous, and these techniques have limitations with respect to producing a homogenously thick layer in the case of complex shaped interconnects [5]. In contrast, electrodeposition of metallic layers followed by thermal treatment to obtain thermally-grown spinel coatings on metallic substrates has been recognized as an advantageous method for preparing spinel coatings. This is attributed to the advantages of the electrodeposition method in comparison with the slurry method. In particular, the electrodeposition method yields better coating-substrate bonding, a denser spinel layer, uniform layers on complex shaped substrates, and easier control of the thickness of the spinel [5,6].

Thus far, few investigations have concentrated on the co-electrodeposition of Co-Mn alloy coatings because of the large difference of standard electrode potentials between Co^{2+}/Co and Mn^{2+}/Mn ($E_0(Mn^{2+}/Mn)$=-1.42 V_{SCE}, $E_0(Co^{2+}/Co)$=-0.521 V_{SCE}) [14,15]. In principle, the addition of proper complexing agents into the electrolyte bath decreases the deposition potential difference between Co^{2+}/Co and Mn^{2+}/Mn, making Co-Mn electrodeposition possible. EDTA and gluconate have been used to improve the Mn-Sn electrodeposition, which also has a large potential difference [16]. The addition of gluconate to a sulfate bath enabled the Co-Mn electrodeposition; however, the deposited Co-Mn coatings had pores and cracks [11,12].

In our previous work, the Co-Mn electrodeposition was enabled by adding EDTA to a chloride bath, and a dense and adhesive Co-Mn coating was successfully prepared [10]. However, the electrochemical process of Co-Mn electrodeposition is still not clear. Therefore, the present work was performed to study the effects of the EDTA additive on the electrodeposition process using modern electrochemical analysis techniques including cyclic voltammetry (CV), potentiodynamic polarization, and anodic linear sweep voltammetry (ALSV).

2. EXPERIMENTAL

Ferritic stainless steel 430 (denoted as 430ss) was used to prepare working electrodes, and its chemical compositions are described elsewhere [10]. Each 430ss coupon had dimensions of 10×10×2 mm and was molded in epoxy with only one face exposed. The molded working electrodes were then mechanically ground to 2000 mesh with silicon carbide papers, polished to a mirror finish, pickled in a

mixed acid solution (containing 5% nitric acid and 25% hydrochloric acid), and then activated in 10% sulfuric acid.

A chloride solution containing 0.05 M $CoCl_2$, 1.25 M $MnCl_2$, 30 g NH_4Cl, 20 g NH_4Br was used as the base electrolyte, where NH_4Br was used to inhibit the evolution of chlorine and oxygen on the anode. For single metal deposition, the bath contained the respective metal salt. Different concentrations of EDTA (0 M, 0.025 M, 0.05 M and 0.1 M) were prepared by adding ethylenediaminetetraacetic acid disodium salt into the base electrolyte. For each test electrolyte, the pH value was adjusted to 4.5. All solutions were prepared using deionized water and analytical grade reagents.

Electrochemical tests were carried out in a PARSTAT 4000 electrochemical workstation using a traditional three-electrode system. A saturated calomel reference electrode (SCE) with saturated potassium chloride solution was used as the reference electrode. A platinum foil was used as the auxiliary electrode. Cathodic potentiodynamic curves were recorded at a scan rate of 1 mV/s. CV curves were obtained by initially scanning toward negative potentials under a rate of 20 mV/s. Stripping analysis was performed as follows: after potentiostatic deposition on the working electrode for 30 s within the potential range -1.6 V ~ -2.1 V, stripping tests were immediately carried out under a scan rate of 20 mV/s. During all of the electrochemical tests, the temperature was maintained at 25 °C, and neither a purge gas nor a stirring treatment were used.

A series of potentials (-1.1 V ~ -1.9 V) were applied to prepare Co-Mn deposits for 300 s. After that, the surface morphology and chemical compositions of the Co-Mn deposits were analyzed using a scanning electron microscope (SEM, FEI INSPECT F50) equipped with an energy dispersive spectrometer (EDS, OXFORD X-Max).

3. RESULTS AND DISCUSSION

Cobalt ion in electrolytes is usually considered to be the divalent cobaltous ion with octahedral coordination [17]. In electrolytes, ammonia molecules generated from ammonium salts can replace water molecules in the coordination octahedron of cobalt because of its preferable coordination with nitrogen. Cobaltous ammines containing 1~6 ammonia molecules can form depending on the concentration and pH of ammonia [15,18]. In the pH range of 0~7, cobalt-ammonia complexes can be ignored, and the cobalt ion mainly exists as an aquo complex, $Co(H_2O)_6^{2+}$ [18]. Manganese ion has octahedral coordination, and in an aqueous solution, it exists mainly as $[Mn(H_2O)_6]^{2+}$ at pH 2.4~4.4 and as $[Mn(H_2O)_{6-n}(NH_3)_n]^{2+}$ at pH 4.4~6.4 [19,20]. With these considerations, ammonia mainly acts as a buffer at the studied pH value of 4.5 in the present work.

For the general reaction shown in Eq. (1), the equilibrium electrode potential can be calculated theoretically according to the Nernst equation, as shown by Eq. (2). E^0 is the standard electrode potential, R is the ideal gas constant, T is the temperature in Celsius, F is the Faraday constant, M represents the metal or metal complex, z is the number of electrons in the electrode reaction, and $a(M^{z+})$ is the ionic activity.

$$M = M^{z+} + z\text{e} \qquad\qquad (1)$$

$$E = E^0 + (RT/zF) \ln a(M^{z+}) \qquad (2)$$

During the process of individual cobalt deposition, Eqs. (3)-(5) may occur, where H_4L is used to represent EDTA. Theoretical calculations according to the Nernst equation indicate that the cobalt deposition potential in the electrolyte without the addition of EDTA is -0.521 V and that the value of the deposition potential in the electrolyte with the addition of EDTA is -1.02 V.

$$Co = Co^{2+} + 2e^- \qquad (3)$$
$$Co^{2+} + H_2L^{2-} = CoL^{2-} + 2H^+ \qquad (4)$$
$$Co + L^{4-} = CoL^{2-} + 2e^- \qquad (5)$$

In the case of single manganese deposition, Eqs. (6)-(8) may occur. According to the Nernst equation, the calculated manganese deposition potential in the electrolyte without the addition of EDTA is -1.424 V, and the value of the deposition potential in the case containing EDTA is -1.838 V.

$$Mn = Mn^{2+} + 2e^- \qquad (6)$$
$$Mn^{2+} + H_2L^{2-} = MnL^{2-} + 2H^+ \qquad (7)$$
$$Mn + L^{4-} = MnL^{2-} + 2e^- \qquad (8)$$

3.1 Effects of EDTA on single metal (Co, Mn) deposition

Fig. 1 shows the cathodic potentiodynamic curves of single cobalt deposition using aqueous chloride electrolytes containing 0 M~0.1 M EDTA. It is evident that the deposition potential of cobalt depends on the concentration of EDTA. With an increase in the concentration of EDTA from 0 M to 0.1 M, the deposition potential of cobalt shifts negatively from -0.87 V to -1.1 V because of the formation of cobalt-EDTA complexes; this shows a trend similar to that of the theoretical calculations using the Nernst equation. The addition of EDTA also reduces the limiting current of cobalt deposition. With an increase in the concentration of EDTA, more cobalt ions become complexed.
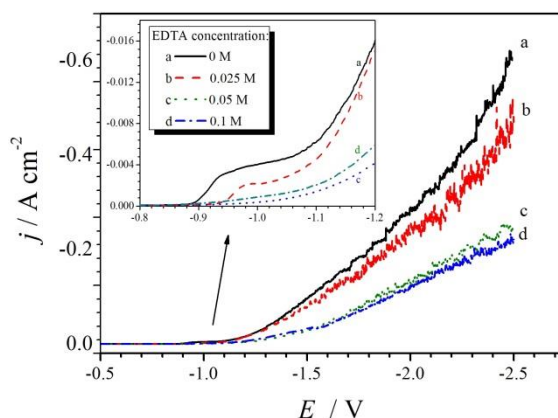

Figure 1. Potentiodynamic curves of 430ss in 0.05 M $CoCl_2 \cdot 6H_2O$ + 30 g·L^{-1} NH_4Cl + 20 g·L^{-1} NH_4Br solutions with different concentrations of EDTA.

At the same concentration, the diffusion coefficient of CoL^{2-} is lower than that for Co^{2+}, and thus the charge transfer reaction rate of Co^{2+} is faster than that for CoL^{2-}. Therefore, the complexation

of EDTA leads to the mass transport of cobalt ions becoming the rate-controlling step. Increasing the concentration of EDTA reduces the concentration of uncomplexed Co^{2+}, and thus the current plateau decreases [21,22]. In the case of equal concentrations of EDTA and cobalt ions in solution (addition of 0.05 M EDTA), most of the cobalt ions become complexed, and the complexation reaction rate tends to diminish. As a result, the current plateau of the cathodic potentiodynamic curve c in Fig. 1 disappears. As indicated by curve d in Fig. 1, for the electrolyte containing 0.1 M EDTA, no further significant shift of the deposition potential (-1.1 V) is seen compared to that in the electrolyte containing 0.05 M EDTA. In sum, increasing the concentration of EDTA in the electrolyte decreases the total partial current density for cobalt deposition and shifts the cobalt deposition potential negatively. Furthermore, addition of EDTA in concentrations greater than 0.05 M EDTA enables the complete complexation of cobalt ions with EDTA.

Fig. 2 presents the potentiodynamic cathodic polarization curves for the single manganese deposition. It can be seen that the deposition potentials decrease with an increase in the EDTA concentration, and this is similar to the trend indicated by the theoretical calculations using the Nernst equation. However, the decreasing trend is much smaller than that for single Co deposition. Addition of 0.1 M EDTA causes only a small negative shift of about 30 mV for the deposition potential of single manganese because of the small ratio of [EDTA]/[Mn^{2+}]. It is worth noting that the presence of EDTA promotes cathodic polarization. With this consideration, EDTA can act as an inhibitor because of its complexation with manganese ions [19]. It is also found that the deposition potential of single manganese is more negative than that of the hydrogen evolution reaction. Therefore, the concentration of EDTA in the electrolytes should be controlled to be as small as possible to avoid the cathodic polarization of manganese.

It can be speculated from the above results that the addition of EDTA into bath electrolytes makes the deposition potentials of single cobalt and manganese closer to one another and that 0.05 M is the most proper concentration of EDTA in the range of concentrations studied herein.
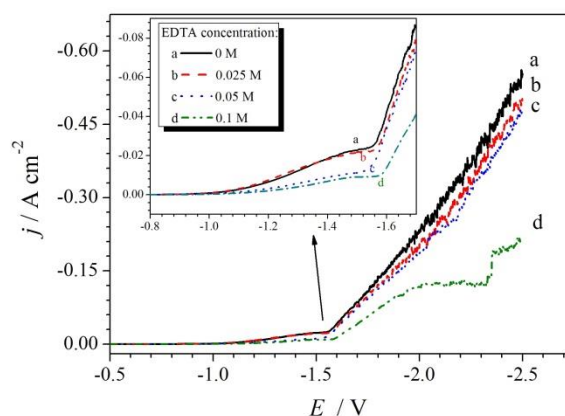

Figure 2. Potentiodynamic behavior of 430ss in 0.05 M $MnCl_2 \cdot 4H_2O$ + 30 g·L^{-1} NH_4Cl + 20 g·L^{-1} NH_4Br solutions with different concentrations of EDTA.

Fig. 3 shows the CV curves of single cobalt deposition. Peak $I_{a,i}$, peak $I_{c,i}$, and peak $II_{c,i}$ represent the first anodic peak, first cathodic peak, and second cathodic peak, respectively, of curve i. Figs. 3b and 3c show the magnified images for the marked areas in Fig. 3a.
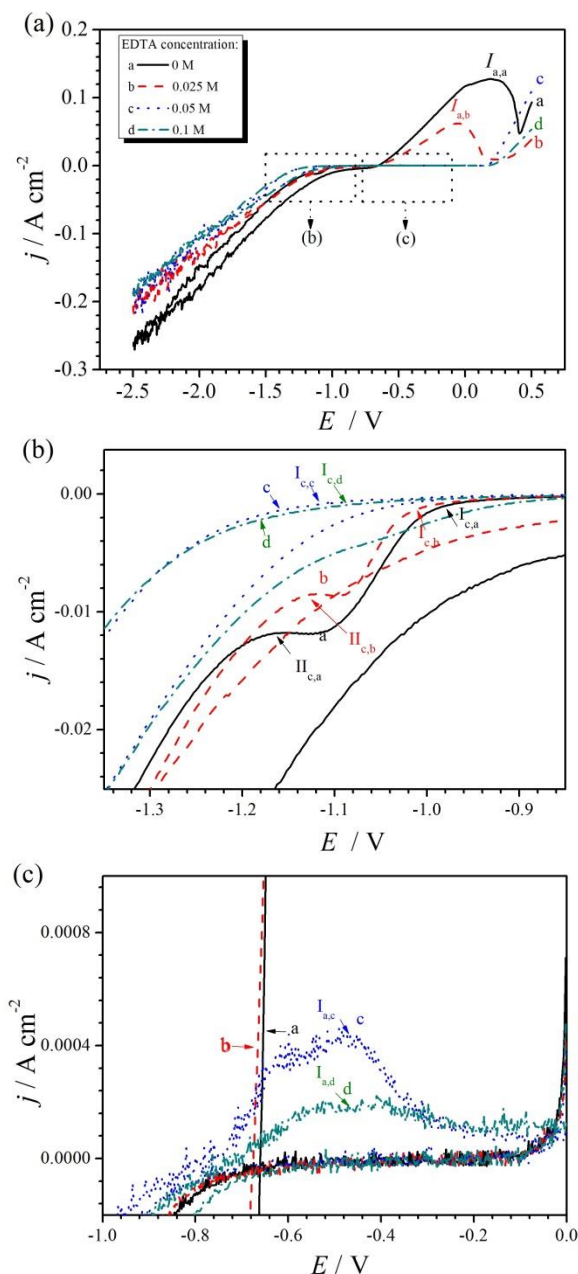

Figure 3. Cyclic voltammograms of 430ss in 0.05 M $CoCl_2 \cdot 6H_2O$ + 30 g·L^{-1} NH$_4$Cl + 20 g·L^{-1} NH$_4$Br solutions with different concentrations of EDTA: (a) general curves; (b) and(c) magnified images corresponding to the marked areas in (a).

In the electrolyte without added EDTA (curve a), it can be seen that there is no reaction in the range of 0 V ~ -1.0 V; however, the cathodic current begins to increase at -1.0 V and results in the presence of peak $I_{c,a}$ (Fig. 3b), which represents the reduction reaction of cobalt. The nucleation overpotential results in the difference between the equilibrium potential of the cobalt redox reaction

and the onset potential of cobalt deposition [17]. This indicates that extra energy is required to overcome the barrier of heterogeneous deposition.

When the negative potential is increased as high as -1.15 V, the second current peak, $II_{c,a}$, (Fig. 3b) appears, corresponding to the hydrogen formation reaction [15]. When the scan is reversed at -2.5 V, the current decays but remains cathodic until -0.7 V, indicating further reduction of the cobalt species. From -2.5 V to -0.7 V, the current in the backward sweep is higher than that in the forward sweep. From these observations, it is suggested that the energy required for cobalt deposition on the cobalt film is lower than that on the bare substrate during the forward sweep [15]. When the potential becomes more positive, the current tends to be anodic and then forms peak $I_{a,a}$ with a current density of 0.127 A/cm^2.

In the electrolyte containing 0.025 M EDTA (curve b), the cyclic voltammogram shows a similar trend to that in the electrolyte without the addition of EDTA (curve a). The first cathodic peak, $I_{c,b}$, lies at -1.02 V, corresponding to the reduction reaction of cobalt ions with partial EDTA complexation. The second cathodic peak, $II_{c,b}$, lies at -1.15 V and corresponds to the reduction reaction of hydrogen ions. The potential at $I_{c,b}$ is possibly related to the concentration overpotential. A lower reactant concentration causes a more negative concentration overpotential [17, 23]. The addition of 0.025 M EDTA causes partial complexation of cobalt ions so that the concentration of isolated cobalt ions is lower, which then causes a more negative potential at peak $I_{c,b}$. When the concentration of EDTA is increased further, more cobalt ions are complexed, and this leads to more negative potential at peak I_c, which overlaps with hydrogen ion reduction, as indicated by $I_{c,c}$ and $I_{c,d}$ in Fig. 3b. For the reverse scan in the electrolyte with added EDTA, the current densities of the peaks $I_{a,b}$ (Fig. 3a), $I_{a,c}$ (Fig. 3c), and $I_{a,d}$ (Fig. 3c) are 0.062 A/cm^2 (0.025 M), 4.4×10^{-4} A/cm^2 (0.05 M), and 2.0×10^{-4} A/cm^2 (0.1 M), respectively. The current density of peak I_a decreases proportionally with the increase in the concentration of EDTA. Also, the pre-deposition of cobalt on the substrate during the anodic stripping process affects the values of I_a. For the prevailing conditions, the anodic stripping charge (the area under the peak) can be used as a qualitative measure of the amount of cobalt deposited [24]. It can be speculated that the amount of cobalt deposition in the electrolyte with 0.025 M EDTA is smaller than that without the addition of EDTA because of the lower amount of cobalt ions after complexation with EDTA. When the concentration of EDTA is greater than 0.05 M, weak peaks can be observed because the cobalt ions are completely complexed with EDTA. Based on the above discussion, concentrations greater than 0.05 M EDTA should be added to ensure that the content of free cobalt ions in the solution is low enough to obtain a Co-Mn alloy coating that has high Mn content.

Fig. 4 shows the CV curves for the single manganese deposition. In all of the cases, there are three main features for the cathodic part: First, the first cathodic peak, I_c, at -0.9 V can be observed and corresponds to the reduction of hydrogen ions. Second, the second cathodic peak, II_c, at -1.6 V can be observed and corresponds to the reduction of manganese ions. Third, the total current density decreases with an increase in the EDTA concentration. This trend can be interpreted to mean that there was a great deal of competition between the electrochemical reaction of the manganese species at the electrode surface as shown by reaction (6) and the homogeneous reaction (7). As the concentration of EDTA increases, the electrochemical reaction of Mn^{2+} decreases significantly, and the partial current density of the complexed manganese species increases slightly. Thus, the overall current density

decreases with an increase in the concentration of EDTA. For the anodic part, it can be seen that an anodic peak, I_a, appears at -1.18 V, corresponding to the dissolution of manganese. As the concentration of EDTA increases, the current peak I_a decreases. Podlaha et al. [21] investigated the deposition of nickel-rich alloys and proposed that, in the case of high current density, the nickel deposit would be principally due to the uncomplexed nickel ions. Based on this model, the partial current density for manganese deposition would be mainly due to the uncomplexed manganese ions. Moreover, the cover area of the anodic peak I_a represents the amount of manganese deposition on the substrate in the previous reduction process. As the concentration of EDTA increases, the concentration of manganese ions decreases, and the amount of deposited manganese is reduced. In all of the cases, the cover area of peak $I_{a,d}$ is the smallest, and this may be ascribed to the low concentration of reacting manganese species. Therefore, to improve the Mn content in the Co-Mn alloy coating, the amount of EDTA should be decreased.
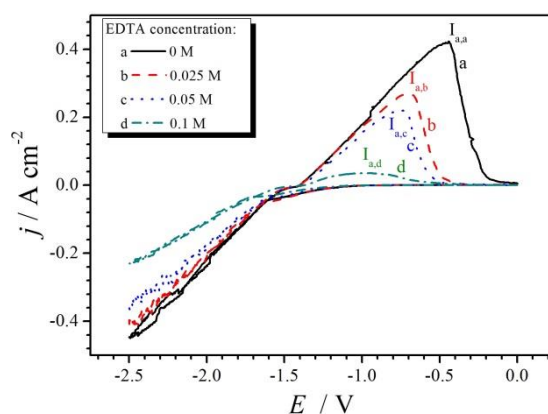

Figure 4. Cyclic voltammograms of 430ss in 1.25 M $MnCl_2 \cdot 4H_2O$ + 0.05 M $CoCl_2 \cdot 6H_2O$ + 30 $g \cdot L^{-1}$ NH_4Cl + 20 $g \cdot L^{-1}$ NH_4Br solutions with different concentrations of EDTA.

From the above results and discussion, it is evident that the influence of EDTA on the electrodeposition potential for single cobalt deposition is much more significant than that for single manganese deposition when the ratio of $[Mn^{2+}]/[Co^{2+}]$ is 25. For the Co-Mn alloy deposition, it is necessary to reduce the formation of complexed manganese ions to bring the deposition potentials between cobalt and manganese much closer. On the other hand, the logarithm of the cumulative stability constant of EDTA complexing with Mn^{2+} (13.8) is smaller than that with Co^{2+} (16.31) [25]. When the ratio of $[Co^{2+}]/[EDTA]$ is one and the complexation of EDTA with cobalt is assumed to be the major reaction, the deposition of a Co-Mn alloy with high Mn content can be achieved. In the present electrolyte bath, the most proper concentration of EDTA is 0.05 M.

3.2 Effects of EDTA on Co-Mn alloy deposition

Fig. 5 presents the CV curves for the Co-Mn alloy deposition. In the electrolyte without the addition of EDTA (curve a), the current peak, $I_{c,a}$, appears at -0.9 V and corresponds to the reduction of

cobalt ions; as the potential becomes more positive, the second peak, $II_{c,a}$, appears at -1.1 V and corresponds to the reduction of hydrogen ions. In the reverse scan, a slight change in the current slope can be observed at -1.0 V and corresponds to the oxidation of hydroxyl ions. As the scan proceeds, the first current peak, $I_{a,a}$, appears at -0.7 V and indicates the oxidation of cobalt. The current becomes anodic and decays at the end of the scan, indicating that cobalt deposition controls the whole deposition period. This is similar to the findings reported in Ref. [26], where Co-Mn alloys prepared from a simple acidic sulfate bath contained a small amount of manganese (2%).
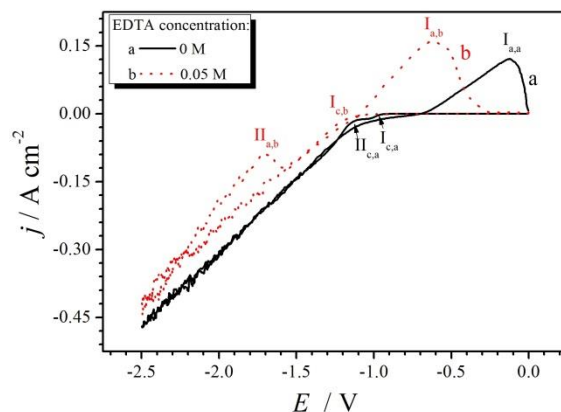

Figure 5. Cyclic voltammograms of 430ss in 1.25 M $MnCl_2 \cdot 4H_2O$ + 0.05 M $CoCl_2 \cdot 6H_2O$ + 30 g·L^{-1} NH_4Cl + 20 g·L^{-1} NH_4Br solutions with different concentrations of EDTA.

In the electrolyte containing 0.05 M EDTA (curve b), the cathodic current peak $I_{c,b}$ appears at -1.15 V and corresponds to the overlapping of hydrogen reduction and cobalt deposition. As the potential becomes more negative, the slope does not change because the major contribution to the current is ascribed to the reduction reaction of hydrogen ions. Also, the deposition of cobalt is controlled by the migrating process, but the deposition of manganese is not. As a result, the slope of the total current, which consists of manganese deposition, hydrogen ion reduction, and cobalt deposition, does not change. In the reverse scan, the anodic current peaks $I_{a,b}$ and $II_{a,b}$ lie at more negative potential. The anodic current peak, $I_{a,b}$, at -1.1 V indicates manganese oxidation. It can be speculated that both manganese deposition and cobalt deposition happen in the electrolyte that has the addition of 0.05 M EDTA. However, the onset potential of the Co-Mn deposition and the reaction peak $II_{a,b}$ are not clear in curve b. The increasing current density leads to a significant increase in the concentration of hydroxyl ions at the deposition/electrolyte interface. Thus, large amounts of manganese hydroxide precipitate and are incorporated into the growing deposition layer [20]. On the other hand, the more negative potential of the manganese deposition compared to that of the hydrogen reduction results in the presence of manganese hydroxide in the deposition before the codeposition of Co-Mn.

Conventional ex situ characterization techniques (e.g., SEM, X-ray diffraction, Auger spectroscopy, etc.) are difficult and time-consuming to use for characterizing electrodeposited alloys [27,28]. More recently, the ALSV technique has been used to identify metallic alloy phases in situ [29]. In principle, ALSV of the dissolution of solid solution should have two or more separate peaks:

one at more negative potential, corresponding to the preferential dissolution of the less noble component, and the second at more positive potential, corresponding to the dissolution of the more noble component [30]. With this consideration, ALSV was used to analyze the reaction mechanism at peak $II_{a,b}$ in Fig. 5.

Fig. 6 shows the ALSV results recorded with a scan rate of 20 mV·s^{-1}. In each case, the scan proceeded from a given potential to 0 V. With the overpotential between -1.6 V and -1.7 V, a single peak appears and indicates the single deposition of cobalt (curve a). However, at more negative potential (-1.8 V), two peaks appear: the first peak, I_{a1}, at -1.1 V corresponds to the dissolution of manganese, and the second peak, I_{a2}, at -0.65 V corresponds to the dissolution of cobalt. This indicates that the codeposition of Co-Mn begins at -1.7 V~-1.8 V and follows a normal type of deposition. With an overpotential of -1.9 V, there are two oxidation peaks, indicating the dissolution of both cobalt and manganese. Also, the oxidation peak of manganese at -1.9 V is larger than that at -1.8 V, indicating a larger amount of manganese at that potential. With an overpotential of -2.0 V, three peaks can be seen, two of which correspond to the dissolution of cobalt and manganese, and the third (at -1.75 V) indicates another reaction at -1.9 V ~ -2.0 V. With an overpotential of -2.1 V, two peaks appear: peak I_a is the overlap of I_{a1} and I_{a2}, and peak II_a is similar to that observed with an overpotential of -2.0 V. By comparing I_{a1} in the various curves, it is observed that the manganese content in the alloy deposit increases when the potential shifts negatively.
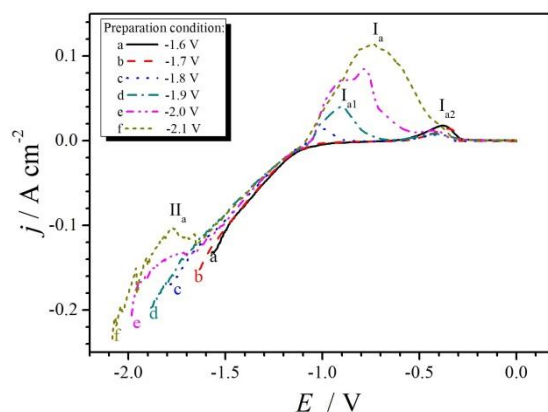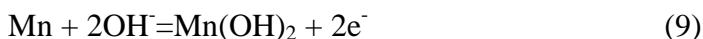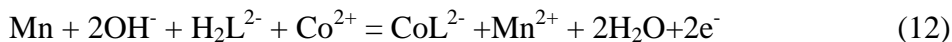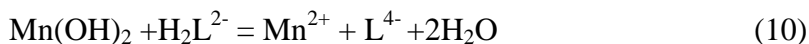

Figure 6. Anodic linear stripping voltammograms of 430ss in 1.25 M MnCl$_2$·4H$_2$O + 0.05 M CoCl$_2$·6H$_2$O + 0.05 M EDTA + 30 g·L^{-1} NH$_4$Cl + 20 g·L^{-1} NH$_4$Br at various potentials for 30s.

Peak $II_{a,b}$ appears only when the cobalt ion, manganese ion, and EDTA are simultaneously present in the electrolyte bath. In such a case, reactions (9)-(12) take place. First, the oxidation of manganese occurs and forms a passivating manganese hydroxide film according to reaction (9), and this corresponds to peak II_a. Second, the manganese hydroxide in the film reacts with H_2L^{2-} and produces soluble manganese chloride and L^{4-} according to reaction (10). Third, the cobalt ion reacts with L^{4-} and forms a Co-EDTA complex according to reaction (11). The complexation of cobalt ions enables reaction (9) to proceed and then to generate the anodic peak II_a. Thus, the overall reaction can be written as reaction (12).

$$Mn + 2OH^- = Mn(OH)_2 + 2e^- \hspace{2cm} (9)$$

$$Mn(OH)_2 + H_2L^{2-} = Mn^{2+} + L^{4-} + 2H_2O \qquad (10)$$
$$Co^{2+} + L^{4-} = CoL^{2-} \qquad (11)$$
$$Mn + 2OH^- + H_2L^{2-} + Co^{2+} = CoL^{2-} + Mn^{2+} + 2H_2O + 2e^- \qquad (12)$$

The presence of peak II_a also indicates that the codeposition of Co-Mn is not the combination of each single metal deposition. The reactions are coupled via a complexing equilibrium and a mass transport process, the latter of which determines the relative concentrations of the complexed and uncomplexed reactants at the electrode surface [21].
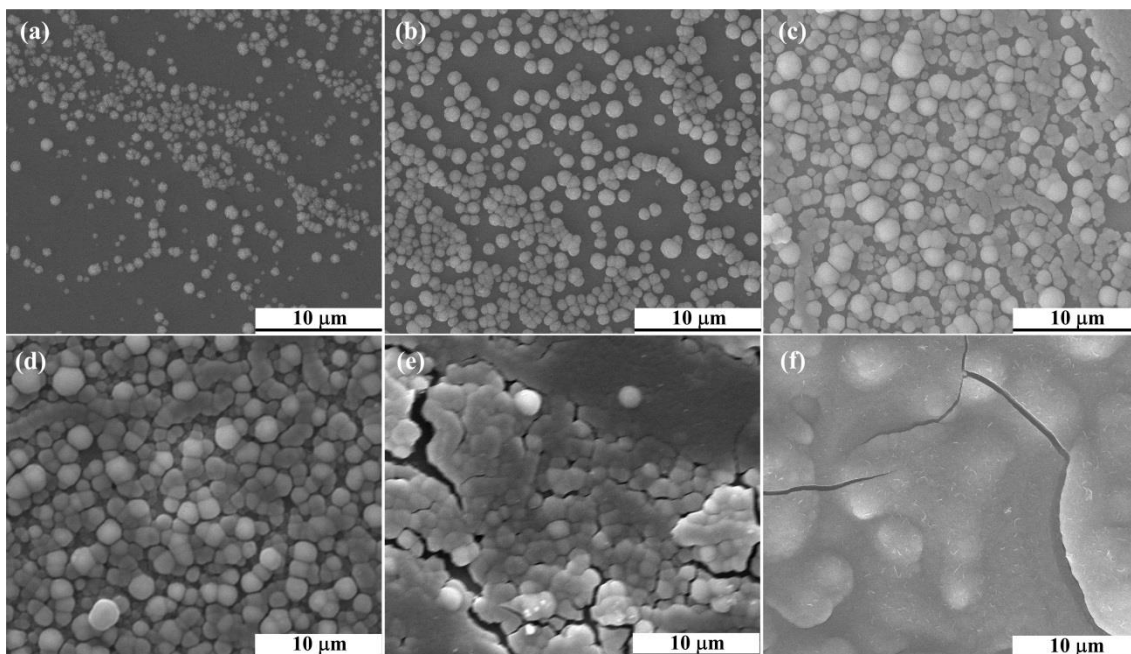

Figure 7. Surface morphology of the Co-Mn alloy deposits prepared in 1.25 M MnCl$_2$·4H$_2$O + 0.05 M CoCl$_2$·6H$_2$O + 0.05 M EDTA + 30 g·L^{-1} NH$_4$Cl + 20 g·L^{-1} NH$_4$Br after 300 s under various potentials: (a) -1.1 V, (b) -1.3 V, (c) -1.5 V, (d) -1.6 V, (e) -1.7 V, and (f) -1.9 V.
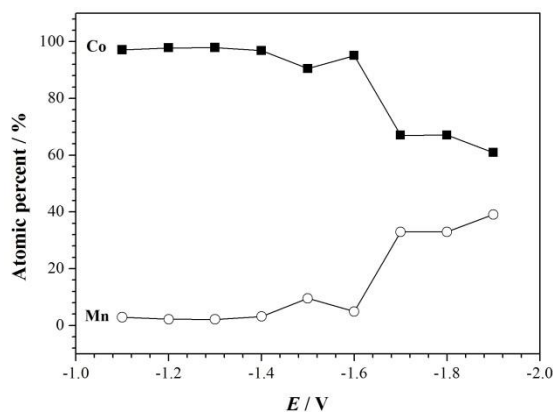

Figure 8. Relative atomic percentages of elements in the Co-Mn deposits prepared in 1.25 M MnCl$_2$·4H$_2$O + 0.05 M CoCl$_2$·6H$_2$O + 0.05 M EDTA + 30 g·L^{-1} NH$_4$Cl + 20 g·L^{-1} NH$_4$Br under various potentials for 300 s.

Fig. 7 presents the surface morphologies of the Co-Mn alloy after electrodeposition under various potentials for 300 s, and Fig. 8 shows the relative atomic percentages of elements in the Co-Mn deposits. In the cases where the applied potential is more positive than -1.6 V, the cobalt particles appear on the metallic surface and tend to be denser as the applied potential increases. In the cases where the applied potential is more negative than -1.7 V, the Co-Mn deposits had cracks and less particles. In addition, it is evident that the Mn content in the deposits remains low enough when the applied potential is more positive than -1.6 V; however, it increases significantly when the applied potential is more negative than -1.7 V. This clearly indicates the deposition of the Co-Mn alloy in the present electrolyte with the addition of EDTA. However, the Co-Mn alloy deposits contain considerable cracks. This may be caused by hydrogen evolution because of the rather negative applied potential, and thus poor performances result. It has been previously reported that several methods, including surface treatment and ultrasonic vibration, can be applied to improve the density and adhesion of deposits [10].

4. CONCLUSIONS

The effects of the EDTA additive on the Co-Mn electrodeposition process were studied using electrochemical technologies, including potentiodynamic polarization, CV, and ALSV. The following conclusions can be made on the basis of the results:

(1) A proper amount of the EDTA additive in the chloride electrolyte brings the discharge potentials between cobalt ions and manganese ions closer, and thus results in Co-Mn electrodeposition in the potential range of -1.7 V ~ -1.8 V.

(2) In the potential range of -1.9 V ~ -2.0 V, a possible reaction ($Mn + 2OH^- + H_2L^{2-} + Co^{2+} = CoL^{2-} + Mn^{2+} + 2H_2O + 2e^-$) occurs, indicating that the codeposition of Co-Mn is not the simple combination of each single metal deposition.

(3) It is crucial to control the ratio of $[Co^{2+}]/[EDTA]$ to form completely complexed cobalt ions and a very small amount of complexed manganese ions and thus to promote the deposition of the Co-Mn alloy.

References

1. T. Brylewski, A. Kruk, M. Bobruk, A. Adamczyk, J. Partyka, P. Rutkowski, *J. Power Sources*, 333 (2016) 145-155.
2. E. D. Wachsman, K. T. Lee, *Science*, 334 (2011) 935-939.
3. H. Falk-Windisch, J. E. Svensson, J. Froitzhein, *J. Power Sources*, 287 (2015) 25-35.

4. D. Ishibashi, S. Taniguchi, Y. Inoue, J. T. Chou, K. Sasaki, *J. Electrochem. Soc.*, 163 (2016) F596-F602.

5. N. Shaigan, W. Qu, D. G. Ivey, W. Chen, *J. Power Sources*, 195 (2010) 1529-1542.

6. J. C.W. Mah, A. Muchtar, M. R. Somalu, M. J. Ghazali, *Int. J. Hydrogen Energ.,* 42 (2017) 9219-9229.

7. Y. Z. Hu, L. L. Yun, T. Wei, C. X. Li, Z. Qi, G. J. Yang, C. J. Li, M. Liu, Int. *J. Hydrogen Energ.,* 41 (2016) 20305-20313.

8. S. Lee, J. Hong, H. Kim, J.-W. Son, J.-H. Lee, B.-K. Kim, H.-W. Lee, K. J. Yoon, *J. Electrochem. Soc.*, 161 (2014) F1389-F1394.

9. J. Pruanen, M. Pihlatie, J. Lagerbom, G. Bolelli, J. Laakso, L. Hyvärinen, M. Kylmälahti, O. Himanen, J. Kiviaho, L. Lusvarghi, P. Vuoristo, *Int. J. Hydrogen Energ.*, 39 (2014) 17284-17294.

10. H. H. Zhang and C. L. Zeng, *J. Power Sources*, 252 (2014) 122-129.

11. J. Wu, Y. Jiang, C. Johnson, X. Liu, *J. Power Sources*, 177 (2008) 376-385.

12. J. Wu, C. D. Johnson, Y. Jiang, R. S. Gemmen, X. Liu, *Electrochim. Acta*, 54 (2008) 793-800.

13. R. Pinto, M. J. Carmezim, M. F. Montemor, *J. Power Sources*, 255 (2014) 251-259.

14. F. Xu, Z. Dan, W. Zhao, G. Han, Z. Sun, K. Xiao, L. Jiang, N. Duan, *J. Electroanal. Chem.*, 741 (2015) 149-156.

15. A. B. Soto, E. M. Arce, M. Palomar-Pardavé, I. González, *Electrochim. Acta*, 41 (1996) 2647-2655.

16. J. Gong and G. Zangari, *Mater. Sci. Eng. A*, 344 (2003) 268-278.

17. D. Grujicic and B. Pesic, *Electrochim. Acta*, 49 (2004) 4719-4732.

18. X. Ji, M. C. Buzzeo, C. E. Banks, R. G. Compton, *Electroanal.*, 18 (2006) 44-52.

19. J. Gong and G. Zangari, *J. Electrochem. Soc.*, 149 (2002) C209-C217.

20. M. Haerifar and M. Zandrahimi, *Appl. Surf. Sci.*, 284 (2013) 126-132.

21. E. A. Podlaha, C. BonhÔte, D. Landolt, *Electrochim. Acta*, 39 (1994) 2649-2657.

22. S. S. A. EI Rehim, S. M. Sayyah, M. M. EI Deeb, *Appl. Surf. Sci.*, 165 (2000) 249-254.

23. E. Gileadi, *Electrode Kinetics for Chemists, Chemical Engineers, and Materials Scientists*, VCH Publishers, (1993) New York, USA.

24. S. S. Abd El Rehin, M. A. M. Ibrahim, M. M. Dankeria, *J. Appl. Electrochem.*, 32 (2002) 1019-1027.

25. S. Kotrlý and L. Sucha, *Handbook of Chemical Equilibria in Analytical Chemistry*, John Wiley & Sons, (1985) New York, USA.

26. S. S. Abd EI Rehim, M. A. M. Ibrahim, M. M. Dankeria, M. Emad, *Trans. Inst. Met. Finish.*, 80 (2002) 105-109.

27. Magdy A. M. Ibrahim, Rasha M. Al Radadi, *Int. J. Electrochem. Sci.*, 10 (2015) 4946-4971.

28. F. Elkhatabi, M. Sarret, C. Muller, *J. Electroanal. Chem.*, 404 (1996) 45-53.

29. A. N. Correia and S. A. S. Machado, *Electrochim. Acta*, 45 (2000) 1733-1740.

30. V. D. Jovic, U. C. Lacnjevac, B. M. Jovic, in *Electrodeposition and surface finishing: Fundamentals and applications,* S. S. Djokic, Editor, Springer, (2014) New York, USA.